Summary and Prognosis. Development of the catalytic cycle in Figure 7 for the Mo-mediated reduction of sulfoxides represents substantial progress in simulating, in a well-defined system, the oxo-transferase activity of reaction 5. For this system, several limitations and reservations are noted. A proposed cycle for enzymatic sulfoxide reduction is presented in Figure 8. Here allowance is made for the likely existence of enzyme complexes of the oxidized and reduced substrate. The most important difference compared to the scheme in Figure 7, however, is the source of electrons for reduction of the enzyme to its active form. A phosphine is obviously a nonphysiological reductant. Current evidence, summarized elsewhere,[10] suggests that the reducing power derives from the indicated $2RSH = RSSR + 2H^+ + 2e^-$ couple of cysteinyl-containing proteins. Consequently, a more physiologically realistic cycle would incorporate this couple. Only *d*-biotin *d*-(S-oxide) reductase, among the biological sulfoxide reducing activities summarized above, has been shown to be a Mo-dependent enzyme. Its purification and structural interrogation of its Mo site will be required before any conclusions can be drawn concerning similarities with $MoO(LNS_2)(DMF)$ and $MoO_2(LNS_2)$. What can be said at this stage of evolution of the oxo-transferase modeling problem is that these complexes are reasonable structural approaches to the catalytic sites of other enzymes of this general type. Further challenges include the development of similarly structurally credible systems capable of the oxo-transfer activities of reactions 1-4.

In the synthetic analogue approach to the active sites of metallobiomolecules, a desirable first step is the attainment of an acceptable *structural* model.[61] It is encouraging to witness recently the development of *reactivity* models for enzyme such as carboxypeptidase A,[62,63] carbonic anhydrase,[64] urease,[65] cytochrome P-450,[66] tyrosinase,[67] and superoxide dismutase.[68] Evolvement of of the sulfoxide reducing system described here, which features substrate saturation kinetics, transformation of the physiological substrate **1**, and a well-defined catalyst capable of turnover of hundreds of equivalents of a model substrate without intervention of a physiologically unrealistic μ-oxo Mo(V) dimer, provides an additional contribution to this endeavor.

Acknowledgment. This research was supported by NSF Grant CHE 81-06017. We thank Don Wink for assistance with the stoichiometric ^{31}P NMR studies.[9]

(61) Ibers, J. A.; Holm, R. H. *Science (Washington, D.C.)* **1980**, *209*, 223.
(62) Breslow, R.; Chin, J.; Hilvert, D.; Trainor, G. *Proc. Natl. Acad. Sci. U.S.A.* **1983**, *80*, 4585.
(63) Groves, J. T.; Chambers, R. R., Jr. *J. Am. Chem. Soc.* **1984**, *106*, 630.
(64) Brown, R. S.; Curtis, N. J.; Huguet, J. *J. Am. Chem. Soc.* **1981**, *103*, 6953. Brown, R. S.; Salmon, D.; Curtis, N. J.; Kusuma, S. *Ibid.* **1982**, *104*, 3188. Slebocka-Tilk, H.; Cocho, J. L.; Frakman, Z.; Brown, R. S. *Ibid.* **1984**, *106*, 2421.
(65) Blakeley, R. L.; Treston, A.; Andrews, R. K.; Zerner, B. *J. Am. Chem. Soc.* **1982**, *104*, 612.
(66) Groves, J. T.; Nemo, T. E. *J. Am. Chem. Soc.* **1983**, *105*, 5786, 6243.
(67) Karlin, K. D.; Cruse, R. W.; Gultneh, Y.; Hayes, J. C.; Zubieta, J. *J. Am. Chem. Soc.* **1984**, *106*, 3372 and references therein.
(68) Strothkamp, K. G.; Lippard, S. J. *Acc. Chem. Res.* **1982**, *15*, 318 and references therein.

Synthesis, Structural Characterization, and Stereospecificity in the Formation of Bimetallic Rhodacarborane Clusters Containing Rh-H-B Bridge Interactions

Paul E. Behnken, Todd B. Marder, R. Thomas Baker, Carolyn B. Knobler, Michael R. Thompson, and M. Frederick Hawthorne*

Contribution from the Department of Chemistry and Biochemistry, University of California, Los Angeles, Los Angeles, California 90024. *Received July 11, 1984*

Abstract: Reactions of $[Rh(COD)(PR_3)Cl]$ (COD = η^4-1,5-cyclooctadiene; R = Ph; Et; Ph, Me) with [*nido*-7-R-7,8-$C_2B_9H_{11}^-$] [R = H, Ph, 7′-*nido*-7′,8′-$C_2B_9H_{11}^-$] resulted in the formation of bimetallic rhodacarborane clusters containing Rh-Rh bonds supported by Rh-H-B interactions. $[Rh(PPh_3)C_2B_9H_{11}]_2$ (**2**) is formed stereospecifically as the nature of the Rh-H-B interactions determines a specific stereoisomer and of the six possible only the structure of **2** is observed. The synthesis, characterization, and X-ray structure determinations of analogues of **2** containing differing phosphine ligands demonstrate this stereospecificity to be of thermodynamic origin, arising from polyhedral repulsions on adjacent carborane ligands. The characterization of $[Rh(PEt_3)_2(H)C_2B_9H_{10}$-$Rh(CODH)C_2B_9H_{10}]$ (**8**) as well as experiments observing the formation of **2** result in a general mechanism for their formation involving hydrogenation of the COD ligand to cyclooctene via phosphine ligand disproportionation. $[Rh(PPh_3)C_2B_9H_{11}]_2$ (**2**) crystallizes in the triclinic space group $P\bar{1}$ with unit cell parameters a = 11.118 (2) Å, b = 13.456 (3) Å, c = 18.390 (3) Å, α = 93.09 (2)°, β = 76.22 (1)°, γ = 76.90 (2)°, Z = 2. $[Rh(PEt_3)C_2B_9H_{10}]_2$ (**3**) crystallizes in the monoclinic space group $P2_1/c$ with unit cell parameters a = 11.153 (6) Å, b = 15.228 (9) Å, c = 18.844 (10) Å, β = 91.83 (2)°, Z = 4. $[Rh(PPh_3)C_2B_9H_{10}C_6H_5]_2$ (**5**) crystallizes in the monoclinic space group $P2_1/c$ with unit cell parameters a = 18.035 (6) Å, b = 13.156 (4) Å, c = 26.905 (8) Å, β = 113.34 (2)°, Z = 4. $[Rh(PEt_3)_2(H)C_2B_9H_{10}$-$Rh(CODH)C_2B_9H_{10}]$ (**8**) crystallizes in the monoclinic space group $P2_1/n$ with unit cell parameters a = 14.043 (7) Å, b = 32.638 (13) Å, c = 10.059 (4) Å, β = 98.98 (3)°, Z = 4.

In the course of our mechanistic study[1] of the homogeneous hydrogenation and isomerization of olefins catalyzed by [*closo*-3,3-(PPh_3)-3-(H)-3,1,2-$RhC_2B_9H_{11}$] (**1**) we reported the structure of a dimeric rhodacarborane, $[Rh(PPh_3)C_2B_9H_{11}]_2$ (**2**), initially

0002-7863/85/1507-0932$01.50/0

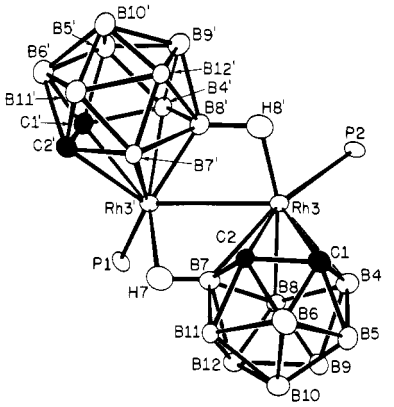

Figure 1. Molecular structure of **2**.

observed as a decomposition product during oxygen-contaminated kinetic experiments involving **1**.[4] We were intrigued by the stereospecificity of the formation of **2**, as six stereoisomers are possible involving isomerization of the Rh–H–B interactions supporting the Rh–Rh bond. Of the six, only the asymmetric structure of **2** was observed.

Subsequently, we reported the structure of $[Rh(PEt_3)C_2B_9H_{10}]_2$[5] (**3**), a bimetallic rhodacarborane analogous to **2** with the two carborane ligands coupled via a single bond between two carbon vertices.[6] The structure of **3** is symmetric (i.e., contains symmetric Rh–H–B interactions) by virtue of the carbon–carbon bond coupling the carboranes which limits these interactions to the boron vertices adjacent to carbon. In this paper we report the synthesis and structures of several more bimetallic rhodacarboranes which allow us to propose not only the origin of the stereospecificity seen in the formation of **2**, but also a general mechanism for the formation of bimetallic species.

Results

We initially reported the synthesis of **2** in moderate yield (40%) by the action of benzoyl peroxide on **1** in refluxing benzene. Subsequently, we discovered a general, high-yield synthesis of **2** employing a reaction between $[Rh(COD)(PPh_3)Cl]$ (COD = η^4-1,5-cyclooctadiene) and $[nido\text{-}7,8\text{-}C_2B_9H_{12}]^-$ (eq 1). The

$$Rh(COD)(PPh_3)Cl + \text{[nido-7,8-}C_2B_9H_{12}\text{]}^- \xrightarrow[\text{Reflux}]{\text{THF}} [Rh(PPh_3)C_2B_9H_{11}]_2 \quad (1)$$

$$\gtrsim 86\%$$

reaction was monitored by ^{31}P NMR spectroscopy and revealed the primary intermediate to be **1**, suggesting that the reaction proceeds via a phosphine disproportionation from the starting $[Rh(COD)(PPh_3)Cl]$, yielding **1** ($2PPh_3$/Rh) and some other specie(s) invisible by ^{31}P NMR spectroscopy. The significance

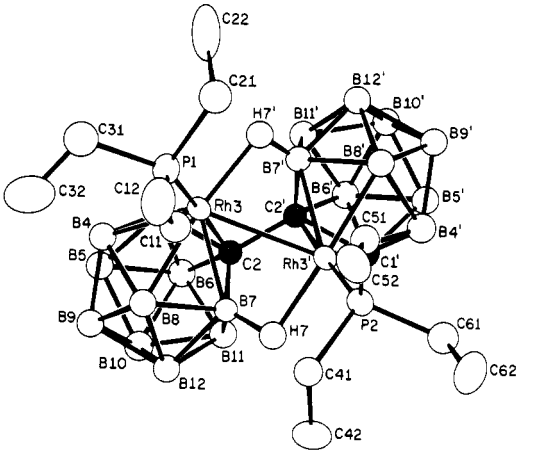

Figure 2. Molecular structure of **3**.

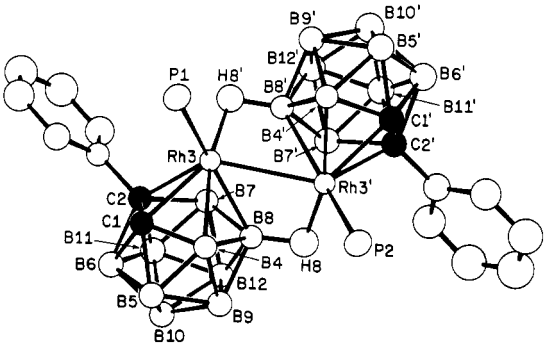

Figure 3. Molecular structure of **5**.

of this observation will be discussed below.

The molecular structure of **2** is shown in Figure 1. The molecule exists as two icosahedral RhC_2B_9 fragments joined by a Rh–Rh bond of 2.763 Å, in the range of a Rh–Rh single bond.[7] The Rh–Rh bond is further supported by two three-center Rh–H–B interactions between Rh3′,H7,B7 and Rh3,H8′,B8′. The rhodacarborane fragments adopt a cis configuration as do the phosphine ligands, and the molecule has a pseudo-two-fold rotation axis which bisects the Rh–Rh bond. The C_2 symmetry is destroyed by the asymmetry of the Rh–H–B interactions. This asymmetry is most readily observed in the $^{31}P\{^1H\}$ NMR spectrum of **2** which exhibits two resonances at 35.4 (J_{Rh-P} = 172 Hz) and 27.8 ppm (J_{Rh-P} = 135 Hz). The resonance at 35.4 ppm also shows an additional 5 Hz of coupling while the upfield resonance is broadened significantly. Selected bond distances and angles for **2** are listed in Table I.

In order to further understand the nature of these Rh–H–B interactions, $[Rh(COD)(PEt_3)Cl]$ was reacted with $Cs_2[7\text{-}(7'\text{-}nido\text{-}7',8'\text{-}C_2B_9H_{11})\text{-}nido\text{-}7,8\text{-}C_2B_9H_{11}]$ (**4**) to produce the bimetallic rhodacarborane $[Rh(PEt_3)C_2B_9H_{10}]_2$ (**3**). We have recently communicated the crystal structure of **3**[6] and an ORTEP projection is depicted in Figure 2.

The structure of **3** consists of two icosahedral rhodacarborane fragments joined at three vertices. C2 and C2′ are covalently bound as in the parent carborane ligand **4**. Rh3 and Rh3′ are attached via a single bond of 2.725 Å, comparable to the Rh–Rh distance in **2**. This bond is further supported by two Rh–H–B interactions between Rh3,H7′,B7′ and Rh3′,H7,B7. Selected bond distances and angles are listed in Table II.

Unlike the asymmetric structure of **2**, the molecule **3** possesses C_2 symmetry with the rotation axis bisecting the Rh3–Rh3′ and C2–C2′ bonds. The carborane ligand adopts a cis configuration about the Rh–Rh bond analogous to that observed in **2**. The $^{31}P\{^1H\}$ NMR spectrum of **3** consists of a sharp doublet at 34.5

(1) Behnken, P. E.; Belmont, J. A.; Busby, D. C.; Delaney, M. S.; King, R. E., III; Kreimendahl, C. W.; Marder, T. B.; Wilcynski, J. J.; Hawthorne, M. F. *J. Am. Chem. Soc.* **1984**, *106*, 3011.

(2) Names for the bimetallacarboranes described in this paper have been assigned according to the descriptor system of Powell et al.[3] In order to avoid ambiguity in discussions of positional isomerism of Rh–H–B interactions, however, the older IUPAC numbering system for *closo*-polyboron hydrides is used in the text, which results in similar numbering schemes for all carborane fragments (i.e., B(8) is always the central boron vertex on the upper pentagonal array of the icosahedral carborane fragment). Thus complex **2** is described[3] as 1,1′-bis(triphenylphosphine)[3,4,4′5′-tetracarba-1,1′-dirhoda[(12*v*)[I_h-(1551)-Δ^{20}-*closo*]-(1:1′)(1,2-di-μH-2′,1′)(12*v*)[I_h-(1551)-Δ^{20}-*closo*]tetracosaborane]](22).

(3) Casey, J. B.; Evans, W. J.; Powell, W. H. *Inorg. Chem.* **1984**, *23*, 4132.

(4) Baker, R. T.; King, R. E. III; Knobler, C.; O'Con, C. A.; Hawthorne, M. F. *J. Am. Chem. Soc.* **1978**, *100*, 8266.

(5) 2,2′-Bis(triethylphosphine)[1,1′,6,6′-tetracarba-2,2′-dirhoda-[(12*v*)[I_h-(1551)-Δ^{20}-*closo*]-(1:1′;2:2′)(2,3-di-μH-3′,2′)(12*v*)[I_h-(1551)-Δ^{20}-*closo*]tetracosaborane]](20).

(6) Behnken, P. E.; Knobler, C. B.; Hawthorne, M. F. *Angew. Chem., Int. Ed. Engl.* **1983**, *22*, 722.

(7) Cotton, F. A.; Felthouse, T. R. *Inorg. Chem.* **1981**, *20*, 584.

Table I. Selected Bond Distances and Angles for Complex **2**

		Bond Distances (Å)	
Rh(03)–Rh(03′)	2.763 (1)	Rh(03)–P(2)	2.338 (2)
Rh(03′)–P(1)	2.360 (2)	Rh(03)–H(08′)	1.78 (6)
Rh(03′)–H(07)	1.77 (6)	Rh(03)–B(08′)	2.327 (8)
Rh(03′)–B(07)	2.238 (8)	Rh(03)–C(01)	2.280 (7)
Rh(03′)–C(01′)	2.214 (7)	Rh(03)–C(02)	2.251 (6)
Rh(03′)–C(02′)	2.269 (7)	Rh(03)–B(04)	2.211 (8)
Rh(03′)–B(04′)	2.190 (8)	Rh(03)–B(07)	2.190 (8)
Rh(03′)–B(07′)	2.221 (8)	Rh(03)–B(08)	2.220 (8)
Rh(03′)–B(08′)	2.173 (8)	C(01)–C(02)	1.579 (9)
C(01′)–C(02′)	1.596 (9)	C(02)–B(07)	1.740 (10)
C(02′)–B(07′)	1.731 (10)	B(07)–B(08)	1.830 (10)
B(07′)–B(08′)	1.829 (10)	B(08)–B(04)	1.830 (10)
B(08′)–B(04′)	1.851 (10)	B(04)–C(01)	1.712 (10)
B(04′)–C(01′)	1.730 (10)		
		Bond Angles (deg)	
H(08′)–Rh(03)–P(2)	85 (2)	H(07)–Rh(03′)–P(1)	89 (2)
H(08′)–Rh(03)–Rh(03′)	83 (2)	H(07)–Rh(03′)–Rh(03)	77 (2)
H(08′)–Rh(03)–C(01)	106 (2)	H(07)–Rh(03′)–C(01′)	147 (2)
H(08′)–Rh(03)–C(02)	95 (2)	H(07)–Rh(03′)–C(02′)	109 (2)
H(08′)–Rh(03)–B(04)	143 (2)	H(07)–Rh(03′)–B(04′)	162 (2)
H(08′)–Rh(03)–B(07)	118 (2)	H(07)–Rh(03′)–B(07′)	89 (2)
H(08′)–Rh(03)–B(08)	166 (2)	H(07)–Rh(03′)–B(08′)	113 (2)
P(2)–Rh(03)–Rh(03′)	123.01 (5)	P(1)–Rh(03′)–Rh(03)	114.91 (5)
P(2)–Rh(03)–C(01)	114.2 (2)	P(1)–Rh(03′)–C(01′)	93.2 (2)
P(2)–Rh(03)–C(02)	153.8 (2)	P(1)–Rh(03′)–C(02′)	115.4 (2)
P(2)–Rh(03)–B(04)	88.6 (2)	P(1)–Rh(03′)–B(04′)	103.3 (2)
P(2)–Rh(03)–B(07)	152.6 (2)	P(1)–Rh(03′)–B(07′)	93.2 (2)
P(2)–Rh(03)–B(08)	106.0 (2)	P(1)–Rh(03′)–B(08′)	148.5 (2)

Table II. Selected Bond Distances and Angles for Complex **3**

		Bond Distances (Å)	
Rh(3′)–H(007)	1.85 (7)	Rh(3)–H(007′)	1.92 (7)
Rh(3′)–B(07′)	2.139 (7)	Rh(3)–B(07)	2.155 (6)
Rh(3′)–C(02′)	2.180 (5)	Rh(3)–C(02)	2.205 (5)
Rh(3′)–B(08′)	2.196 (7)	Rh(3)–B(08)	2.189 (7)
Rh(3′)–B(04′)	2.219 (7)	Rh(3)–B(04)	2.219 (7)
Rh(3′)–C(01′)	2.247 (6)	Rh(3)–C(01)	2.258 (6)
Rh(3′)–P(2)	2.287 (2)	Rh(3)–P(1)	2.284 (2)
Rh(3′)–B(07)	2.323 (7)	Rh(3)–B(07′)	2.306 (7)
Rh(3′)–Rh(3)	2.725 (1)	C(02′)–C(02)	1.506 (8)
B(07′)–H(007′)	1.02 (7)	B(07)–H(007)	1.19 (7)
B(07′)–C(02′)	1.759 (8)	B(07)–C(02)	1.784 (8)
B(07′)–B(08′)	1.806 (9)	B(07)–B(08)	1.812 (9)
B(04′)–C(01′)	1.713 (9)	B(04)–C(01)	1.728 (9)
B(04′)–B(08′)	1.842 (10)	B(04)–B(08)	1.856 (10)
C(01′)–C(02′)	1.642 (8)	C(01)–C(02)	1.627 (8)
		Bond Angles (deg)	
H(007)–Rh(3′)–P(2)	84 (2)	H(007′)–Rh(3)–P(1)	88 (2)
H(007)–Rh(3′)–Rh(3)	76 (2)	H(007′)–Rh(3)–Rh(3′)	72 (2)
B(07′)–Rh(3′)–B(07)	97.2 (2)	B(07)–Rh(3)–B(07′)	97.2 (3)
B(07′)–Rh(3′)–P(2)	131.9 (2)	B(07)–Rh(3)–P(1)	129.9 (2)
C(02′)–Rh(3′)–P(2)	178.0 (2)	C(02)–Rh(3)–P(1)	178.1 (2)
B(08′)–Rh(3′)–P(2)	97.1 (2)	B(08)–Rh(3)–P(1)	96.4 (2)
B(04′)–Rh(3′)–P(2)	100.1 (2)	B(04)–Rh(3)–P(1)	101.2 (2)
C(01′)–Rh(3′)–P(2)	134.9 (2)	C(01)–Rh(3)–P(1)	137.7 (2)
P(2)–Rh(3′)–B(07)	108.2 (2)	P(1)–Rh(3)–B(07′)	108.2 (2)
P(2)–Rh(3′)–Rh(3)	115.37 (5)	P(1)–Rh(3)–Rh(3′)	113.62 (5)
B(04′)–H(004′)–Rh(3)	99 (5)	B(04)–H(004)–Rh(3′)	97 (4)

ppm (J_{Rh-P} = 173 Hz), with no smaller coupling observed. The symmetry of the Rh–H–B interactions observed in **3** can be attributed to the C2–C2′ bond which limits these interactions to the boron vertices adjacent to these carbons (B7 and B7′, respectively).

Reaction of [*nido*-7-C_6H_5-7,8-$C_2B_9H_{11}$]$^-$ with [Rh(COD)(PPh_3)Cl] in MeOH resulted in the formation of a new aqua-colored complex which was spectroscopically similar to **2** and **3** and exhibited a broad doublet in its ^{31}P NMR spectrum at 17.6 ppm (J_{Rh-P} = 134 Hz). In order to characterize the nature of the Rh–H–B interactions in this complex, an X-ray crystallographic structure was undertaken, whose results are depicted in Figure 3. The structure of [Rh(PPh_3)$C_2B_9H_{10}C_6H_5$]$_2$[8] (**5**) contains two icosahedral rhodacarborane fragments joined through Rh3–Rh3′ at a distance of 2.791 Å. The complex contains two phenyl substituents on C2 and C2′ which were present in the carborane anion precursor. The Rh–H–B interactions supporting the Rh–Rh bond are symmetrically disposed between Rh3,H8′,B8′ and Rh3′,H8,B8. Similar to complexes **2** and **3**, **5** contains a cis configuration of the two carborane clusters as well as the two phosphine ligands. The presence of symmetric Rh–H–B interactions imparts C_2 symmetry to **5**, like **3**, but differing in that the

(8) 4,4-Diphenyl-1,1′-bis(triphenylphosphine)[4,4′,5,5′-tetracarba-1,1′-dirhoda[(12*v*)[I_h-(1551)-Δ^{20}-*closo*]-(1:1′)(1,2-di-μH-2′,1′)-(12*v*)[I_h-(1551)-Δ^{20}-*closo*]tetracosaborane]](22).

Table III. Selected Bond Distances and Angles for **5**

Bond Distances (Å)			
Rh(03)–Rh(03′)	2.791 (1)	Rh(03′)–P(2)	2.424 (2)
Rh(03)–P(1)	2.410 (2)	Rh(03′)–H(08)	1.653
Rh(03)–H(08′)	1.656	Rh(03′)–B(08)	2.273 (7)
Rh(03)–B(08′)	2.257 (7)	Rh(03′)–C(01′)	2.231 (6)
Rh(03)–C(01)	2.221 (6)	Rh(03′)–C(02′)	2.307 (6)
Rh(03)–C(02)	2.298 (6)	Rh(03′)–B(04′)	2.190 (7)
Rh(03)–B(04)	2.192 (7)	Rh(03′)–B(07′)	2.172 (7)
Rh(03)–B(07)	2.211 (7)	Rh(03′)–B(08′)	2.170 (7)
Rh(03)–B(08)	2.183 (6)	C(01′)–C(02′)	1.604 (8)
C(01)–C(02)	1.613 (8)	C(02′)–B(07′)	1.766 (9)
C(02)–B(07)	1.750 (9)	B(07′)–B(08′)	1.835 (9)
B(07)–B(08)	1.847 (9)	B(08′)–B(04′)	1.842 (9)
B(08)–B(04)	1.822 (9)	B(04′)–C(01′)	1.729 (8)
B(04)–C(01)	1.712 (9)		
Bond Angles (deg)			
H(08′)–Rh(03)–P(1)	87.4	H(08)–Rh(03′)–P(2)	83.0
H(08′)–Rh(03)–Rh(03′)	83.9	H(08)–Rh(03′)–Rh(03)	84.8
H(08′)–Rh(03)–C(01)	145.3	H(08)–Rh(03′)–C(01′)	143.7
H(08′)–Rh(03)–C(02)	106.2	H(08)–Rh(03′)–C(02′)	106.4
H(08′)–Rh(03)–B(04)	162.8	H(08)–Rh(03′)–B(04′)	166.4
H(08′)–Rh(03)–B(07)	87.8	H(08)–Rh(03′)–B(07′)	89.9
H(08′)–Rh(03)–B(08)	144.3	H(08)–Rh(03′)–B(08′)	117.2
P(1)–Rh(03)–Rh(03′)	115.63 (5)	P(2)–Rh(03′)–Rh(03)	115.89 (5)
P(1)–Rh(03)–C(01)	95.0 (2)	P(2)–Rh(03′)–C(01′)	95.6 (2)
P(1)–Rh(03)–C(02)	113.8 (2)	P(2)–Rh(03′)–C(02′)	114.0 (2)
P(1)–Rh(03)–B(04)	106.6 (2)	P(2)–Rh(03′)–B(04′)	107.4 (2)
P(1)–Rh(03)–B(07)	155.9 (2)	P(2)–Rh(03′)–B(07′)	115.9 (2)
P(1)–Rh(03)–B(08)	151.2 (2)	P(2)–Rh(03′)–B(08′)	151.8 (2)

Table IV. Correlation of Phosphine Basicity with Rh–H–B Positional Isomerism Observed in Rhodacarborane Dimers

phosphine	basicity ν,[9] cm^{-1}	cone angle, deg	% asymmetric isomer
PPh_3	2068.9	145	100
PMe_2Ph	2065.3	122	85
PEt_3	2061.7	132	50

interactions in **5** are with the boron vertices (B8 and B8′) opposite, rather than adjacent, to the carbon vertices in the upper pentagonal C_2B_3 array of the carborane ligands. Selected bond distances and angles in **5** are represented in Table III.

The availability of a general route to these bimetallic complexes via reaction of $[Rh(COD)(PR_3)Cl]$ with $[nido\text{-}7,8\text{-}C_2B_9H_{12}]^-$ allowed the preparation of the PMe_2Ph and PEt_3 derivatives of **2** (eq 2 and 3). Substituting the PPh_3 ligand with the increasingly

$$Rh(COD)(PMe_2Ph)Cl + [nido\text{-}7,8\text{-}C_2B_9H_{12}]^- \xrightarrow[\text{Reflux}]{\text{THF}} [Rh(PMe_2Ph)C_2B_9H_{11}]_2 \quad (2)$$

6, 83%

$$Rh(COD)(PEt_3)Cl + [nido\text{-}7,8\text{-}C_2B_9H_{12}]^- \xrightarrow[\text{Reflux}]{\text{THF}} [Rh(PEt_3)C_2B_9H_{11}]_2 \quad (3)$$

7, 76%

basic PMe_2Ph and PEt_3 ligands results in the observation of symmetric bimetallic species. In the case of **6**, the $^{31}P\{^1H\}$ NMR spectrum exhibits resonances characteristic of an asymmetric structure analogous to **2** (7.1 ppm, J_{Rh-P} = 165 Hz, $^3J_{P-P}$ = 10 Hz; 1.2 ppm, J_{Rh-P} = 130 Hz). Additionally, a symmetric isomer exhibiting a sharp doublet at 8.1 ppm is observed with an integrated intensity of 15% of the asymmetrical isomer.

Substitution with the more basic PEt_3 yields **7** which exists as a 50:50 mixture of an asymmetric (25.8 ppm, J_{Rh-P} = 160 Hz, $^3J_{P-P}$ = 8 Hz; 13.7 ppm, J_{Rh-P} = 129 Hz) and a symmetric structure (27.5 ppm, J_{Rh-P} = 157 Hz). The correlation of phosphine basicity and steric requirements[9] (cone angle) with the positional isomerism of the Rh–H–B interactions is summarized in Table IV. Phosphine basicities are tabulated according to the electronic parameter ν (cm^{-1}) described by Tolman,[9] a smaller ν corresponding to a more basic phosphine.

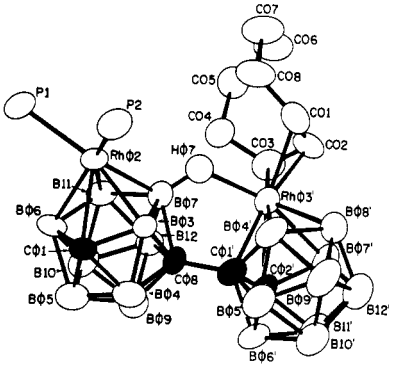

Figure 4. Molecular structure of **8**.

Additionally, we wish to report the other major product in the reaction of $[Rh(COD)(PEt_3)Cl]$ with **4** which resulted in the formation of a new bimetallic species **8**[10] (eq 4). This reaction

$$Rh(COD)PEt_3Cl + [nido\text{-}7,8\text{-}C_2B_9H_{12}]^{2-} \xrightarrow[\text{Reflux}]{\text{THF}} Rh(CODH)C_2B_9H_{10}Rh(PEt_3)_2(H)C_2B_9H_{10} + \underset{\sim}{3}, 23\% \quad (4)$$

8, 19%

produced **3** and **8** in 23% and 19% yields, respectively. Complex **8** was analyzed by X-ray crystallography in order to obtain an unambiguous structural characterization. An ORTEP projection of the results of that study is shown in Figure 4.

(9) Tolman, C. A. *Chem. Rev.* **1977**, *77*, 313.

(10) 2-(1,2,3-η-Cyclooct-1-en-1-yl)-7′,7′-bis(triethylphosphine)[7′*H*-1,1′,3,8′-tetracarba-2,7′-dirhoda[(12*v*)[I_h-(1551)-Δ^{20}-*closo*]-(1:1′)(2,2′-μH)-(12*v*)[I_h-(1551)-Δ^{20}-*closo*]tetracosaborane]](22).

Table V. Selected Bond Distances and Angles for **8**

Bond Distances (Å)			
Rh(02)–P(1)	2.356 (4)	Rh(03′)–C(01)	2.211 (17)
Rh(02)–P(2)	2.347 (5)	Rh(03′)–C(02)	2.109 (15)
Rh(02)–C(01)	2.321 (13)	Rh(03′)–C(03)	2.251 (14)
Rh(02)–B(03)	2.192 (15)	Rh(03′)–C(01′)	2.189 (15)
Rh(02)–B(06)	2.247 (16)	Rh(03′)–C(02′)	2.283 (15)
Rh(02)–B(07)	2.202 (16)	Rh(03′)–B(04′)	2.191 (17)
Rh(02)–B(11)	2.242 (16)	Rh(03′)–B(07′)	2.164 (17)
C(08)–C(01′)	1.510 (18)	Rh(03′)–B(08′)	2.201 (20)
B(07)–H(07)	1.25 (15)	Rh(03′)–H(07)	1.92 (15)
C(01)–C(02)	1.404 (23)	C(02)–C(03)	1.386 (21)
C(03)–C(04)	1.534 (21)	C(04)–C(05)	1.510 (21)
C(05)–C(06)	1.540 (26)	C(06)–C(07)	1.525 (26)
C(07)–C(08)	1.540 (24)	C(08)–C(01)	1.520 (23)

Bond Angles (deg)			
P(1)–Rh(02)–P(2)	98.0 (2)	C(01)–Rh(03′)–C(02)	37.8 (6)
C(01)–Rh(02)–P(1)	118.9 (4)	C(02)–Rh(03′)–C(03)	36.9 (6)
C(01)–Rh(02)–P(2)	103.6 (4)	C(01)–Rh(03′)–C(03)	66.3 (6)
B(03)–Rh(02)–P(1)	162.8 (4)	C(01)–Rh(03′)–H(07)	83 (4)
B(03)–Rh(02)–P(2)	87.1 (4)	C(02)–Rh(03′)–H(07)	104 (4)
B(06)–Rh(02)–P(1)	87.5 (4)	C(03)–Rh(03′)–H(07)	89 (4)
B(06)–Rh(02)–P(2)	142.0 (5)	C(01)–C(02)–C(03)	122 (2)
B(07)–Rh(02)–P(1)	139.0 (4)	C(02)–C(03)–C(04)	124 (1)
B(07)–Rh(02)–P(2)	115.1 (5)	C(02)–C(01)–C(08)	124 (2)
B(11)–Rh(02)–P(1)	96.2 (4)	B(11)–Rh(02)–P(2)	162.3 (5)
B(07)–H(07)–Rh(03′)	121 (9)		

Unlike the previous structures, **8** contains no Rh–Rh bond. The molecule consists of two icosahedral rhodacarborane fragments attached to each other through a pair of carbon vertices and a single Rh–H–B bridge bond. Rh2 is sequestered in a carborane ligand which has undergone a polyhedral rearrangement involving migration of the carbon vertices away from each other. In this case, C8, which is bonded to the adjacent rhodacarborane fragment, has migrated from a position next to C1 and Rh2 to a position on the lower pentagonal array of polyhedral vertices. Rearrangements of this type are common in carborane and metallacarborane chemistry and have been characterized in analogous rhodacarborane systems.[11]

Rh2 is also bound to two triethylphosphine ligands and a terminal hydride which was not located crystallographically but was observed in the ^{1}H NMR spectrum at −10.54 ppm (J_{P-H} = 28 Hz, J_{Rh-H} = 18 Hz). The rhodacarborane fragment bearing Rh2 can be considered analogous to **1**, observed as an intermediate in the formation of **2**.

The other half of the molecule contains Rh3′ bound to a carborane ligand attached through C2′ to C8. Rh3′ is attached to a η^3-cyclooctenyl ligand which can be derived from 1,5-cyclooctadiene via formal migratory insertion into a metal hydride. Insertions of this type open a site of coordinative unsaturation which is occupied by a three-center two-electron interaction between Rh3′, H7, and B7. This Rh–H–B interaction is analogous to those previously discussed which support Rh–Rh bonds. Pertinent bond distances and angles for **8** are listed in Table V. The significance of this structure with respect to the formation of metal–metal bonded species will be discussed below.

Discussion

Three-center two-electron interactions between transition metals and borane and carborane substrates are fairly common and have been structurally characterized in several cases.[12] In the present case, these interactions may be best considered as a two-electron dative bond between an electron-rich boron hydride and an electronically unsaturated transition metal. These bonds are characterized by very broad resonances in the ^{1}H NMR spectra in the range of −4.0 to −9.0 ppm which sharpen slightly at lower temperatures. The ^{11}B NMR resonances characteristic of these interactions are shifted downfield in the range of 5–20 ppm.

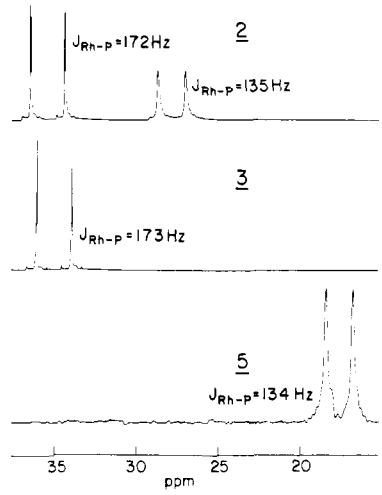

Figure 5. The ^{31}P{^{1}H} NMR spectra of complexes **2**, **3**, and **5** in benzene solution at 25 °C.

The characterization of the complexes reported in this paper allows several points to be addressed with respect to their mode of formation and chemistry. The structural determinations of bimetallic species **2**, **3**, and **5** allow us to propose a correlation between the ^{31}P NMR spectra of these species and their structural conformations (i.e., positions of Rh-H-B interactions). Additionally, the synthesis of complexes analogous to **2** but with differing phosphine ligands (**6** and **7**) and substituents on the carborane ligands (**3** and **5**) yields insight into the unusual stereospecificity seen in the formation of **2**. Finally, in situ experiments which observe the course of the reaction of [Rh(COD)(PPh$_3$)Cl] with [*nido*-7,8-$C_2B_9H_{12}$]$^-$ combined with the structural characterization of **8** result in a general mechanism for metal–metal bond formation via the binuclear hydrogenation of 1,5-cyclooctadiene to cyclooctene.

The ^{31}P{^{1}H} NMR spectra of **2**, **3**, and **5** are illustrated in Figure 5. Complexes **2**, **3**, and **5** represent three distinct classes of rhodacarborane dimers ranging from asymmetric (**2**, by virtue of Rh–H–B interactions discussed) to symmetric {**3**, Rh interactions with B7 and B7′, both adjacent to carbons C2 and C2′, respectively (Figure 2)}. Additionally, **5** has a symmetric structure (Figure 3) involving Rh interactions with B8 and B8′. Inspection of Figure 5 shows that each of these complexes exhibits a characteristic ^{31}P NMR spectrum. Compound **2** has two resonances at 36.7 and 29.7 ppm with J_{Rh-P} = 172 and 135 Hz, respectively. The upfield resonance has significantly larger line widths (ca. 15 Hz), which sharpen only slightly at lower temperatures (200 K). We attribute this to coupling of the ^{31}P nucleus to the quadrupole moments of ^{10}B and ^{11}B nuclei, resulting in more efficient quadrupole-induced relaxation.[13] We can therefore assign this resonance to P1 (Figure 1) which is trans to the B7′–B8′ interaction on the face of the carborane ligand. The sharp downfield resonance at 36.7 ppm is assigned to P2 which is approximately trans to C2 (∠P2–Rh3–C2 = 154°). This resonance also exhibits a small coupling ($^3J_{P-P}$ = 5 Hz) which is unobserved in the resonance at 29.7 ppm, presumably due to its larger line widths. The most compelling argument that this is a P–P coupling is that it is not observed in symmetric structures containing equivalent phosphorus nuclei.

This sensitivity of the ^{31}P NMR resonance to the nature of the polyhedral vertex occupying the trans position about the pseudooctahedral Rh center is also reflected in the magnitude of J_{Rh-P} as ^{31}P resonances trans to boron vertices exhibit smaller values of J_{Rh-P}.[14] This is consistent with our assignment of ^{31}P NMR resonances and allows ^{31}P NMR spectroscopy to be useful in predicting the nature of the Rh–H–B interactions which support the metal–metal bond.

(11) Knobler, C. B.; Marder, T. B.; Mizusawa, E. A.; Teller, R. G.; Long, J. A.; Behnken, P. E.; Hawthorne, M. F. *J. Am. Chem. Soc.* **1984**, *106*, 2990.
(12) Teller, R. G.; Bau, R. *Struct. Bond.* **1981**, *44*, 1.
(13) Bacon, J.; Gillespie, R. J.; Quail, J. W. *Can. J. Chem.* **1963**, *41*, 3063.
(14) Marder, T. B.; Baker, R. T.; Long, J. A.; Doi, J. A.; Hawthorne, M. F. *J. Am. Chem. Soc.* **1981**, *103*, 2988.

Consistent with this correlation are the structures and ^{31}P NMR spectra of **3** and **5**. Complex **3** (Figure 2) has phosphorus atoms trans to C2 and C2′ (∠P–Rh–C = 178.1, 177.9°) and exhibits a sharp resonance at 34.4 ppm with J_{Rh-P} = 173 Hz. Complex **5** (Figure 3) contains PPh_3 ligands trans to the B7–B8 interaction on the respective carborane cluster and accordingly exhibits a broad doublet in its ^{31}P spectrum at 17.6 ppm with J_{Rh-P} = 134 Hz.

In the case of **3**, the symmetric nature of the Rh–H–B interactions can be viewed as a consequence of the C2–C2′ bond which limits these interactions to the adjacent vertices.[6] We propose the symmetry of **5** to result from steric interactions of the phenyl substituents on C2 and C2′ with the phenyl groups on the phosphine ligands as well as the adjacent carborane ligand. Like **2** and **3**, the molecule **5** has a cis configuration of the two carborane fragments as well as the phosphine ligands. Isomerization of the Rh–H–B interaction, which can be viewed as a fivefold rotation of one of the π-bound carborane ligands about the rhodium vertex, would rotate the phenyl substituent on the carborane cluster into either the adjacent carborane cluster or the phenyl groups on the phosphine ligand. This hypothesis was tested by construction of molecular models built from crystallographic data.[15]

Further evidence of steric control of the structural isomerism of **5** originates with the asymmetry of the [*nido*-7-C_6H_5-7,8-$C_2B_9H_{11}$] fragment. The mirror plane symmetry of an unsubstituted [*nido*-7,8-$C_2B_9H_{11}$] fragment is destroyed by substitution on one of the carbons. One might anticipate diastereomers in the formation of dimeric species which differ by the absolute configurations of one of the carborane fragments. In fact, another isomer of **5** is observed in crude reaction mixtures with $^{31}P\{^1H\}$ NMR resonances at 33.1 ppm (J_{Rh-P} = 171 Hz, $^3J_{P-P}$ = 5 Hz) and 22.9 ppm (J_{Rh-P} = 134 Hz) with line widths characteristic of an asymmetric structure analogous to that of **2**. Inversion of configuration of one carborane fragment in the structure of **5** (Figure 3) would result in formal migration of the phenyl substituent from C2 to C1 and an asymmetric structure. If steric considerations were important, these could be relieved via a rotation on the fivefold axis of the carborane ligand, resulting in a structure topologically analogous to **5** but having an asymmetric set of Rh–H–B interactions.

The syntheses of the PMe_2Ph and PEt_3 derivatives of **2**, complexes **6** and **7**, are relevant to the stereospecificity of the formation of **2**. Table IV illustrates the correlation of phosphine ligand basicity with the appearance of symmetric structures analogous to **3** (Rh–H–B interactions to B7 and B7′). Relative phosphine basicities are tabulated according to the electronic parameter ν (cm^{-1}) described by Tolman,[9] a smaller value representing a more basic phosphine. Formation of this isomer would bring C2 and C2′ in close proximity; in fact, these two vertices are covalently bound in **3**. The cis arrangment of carborane ligands in **2** results in close interaction of the two polyhedral vertices adjacent to the boron vertices involved in Rh–H–B interactions. In the structure of **2**, the B7′–C2 distance of 3.174 Å is quite close for a nonbonding interaction. Estimates of the van der Waals radius of carbon range from 1.55 to 1.70 Å[16], resulting in an estimate of the *maximum* van der Waals radius for boron from 1.47 to 1.62 Å, providing no bonding interaction exists between C2 and B7′. The analogous B7–B7′ distance in complex **5** is 3.202 Å.

A characteristic reaction of carboranes and metallocarboranes is polyhedral rearrangements involving migration of carbon vertices away from each other due to accumulation of positive charge on these vertices.[17] We have recently reported the structure of [*closo*-1-(CH_3)-2,2-$(PEt_3)_2$-2-(H)-8-(C_6H_5)-2,1,8-$RhC_2B_9H_9$] which was prepared via polyhedral rearrangement from a tautomeric analogue of **1**.[11] Additionally, complex **8** is formed through an analogous polyhedral rearrangement. In light of the precedent of such rearrangements, we propose the asymmetric structure of **2** to be a consequence of a molecular rearrangement involving repulsion of the C2 and C2′vertices. This is supported by the tendency of more basic phosphine ligands to favor formation of symmetric structures analogous to **3**, as these ligands trans to C2 and C2′ would partially relieve the accumulated charge on these vertices.

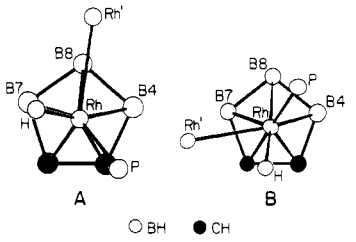

Figure 6. Conformations about Rh observed in bimetallic complexes.

Consequently, we propose the stereospecificity of the formation of **2** to be of thermodynamic rather than kinetic origin. Further evidence for this argument is obtained by photolyzing sealed tubes containing dissolved **2** in benzene, resulting in the observation of a broad doublet at 22.6 ppm (J_{Rh-P} = 134 Hz) and a sharp doublet of lower intensity at 36.4 ppm (J_{Rh-P} = 168 Hz). These chemical shifts and coupling constants are consistent with isomeric forms of **2** analogous to **3** and **5** (both types of symmetric structures). Relaxation of the system results in quantitative conversion of these new isomers back to **2**, demonstrating the thermodynamic stability of the asymmetric structure relative to symmetric conformations.

Disregarding the polyhedral repulsions discussed above, there appears to be an innate preference for Rh–H–B interactions involving H7 and B7. This may result from an energetically more favorable interaction of Rh with H7,B7 than with H8,B8. We have observed a preference for exopolyhedrally bound rhodium centers to interact with B–H vertices adjacent to carbon vertices in the solid state.[11] However, these interactions are with *nido* carborane ligands rather than with *closo*-metallacarborane ligands as in the present case. Alternatively, this may reflect a rotameric preference of the rhodium vertex in the π-bound pentagonal face of the carborane ligand. Extended Hückel molecular orbital studies regarding conformational preferences of $[ML_2]$ and $[ML_3]$ fragments with respect to pentagonal π-systems have been reported by Hoffman et al.[18] and Mingos.[19] Additionally, we have studied the conformational preferences of RhL_2H vertices in substituted [*nido*-7-R-7,8-$C_2B_9H_{11}$] ligands by dynamic NMR.[14] The two conformations of the RhL_3 vertex observed in all isomers of bimetallic complexes are shown in Figure 6. The RhL_3 fragment consists of an asymmetric rhodium bound to another rhodium, a phosphine, and a bridging hydrogen. Conformation A represents the rotameric configuration involving Rh–H–B interactions between Rh′–H8–B8, while conformation B represents interactions between Rh′–H7–B7. The conformations A and B shown are in approximate agreement with the low-energy conformations predicted by dynamic NMR studies,[14] but a qualitative ordering of the relative energies of the two is not possible in this case without reliable calculations. The predicted low energy associated with configurations of A and B may explain the absence of any observed interactions between Rh′ and H4,B4.

Monitoring (in situ) the reaction of [Rh(COD)(PPh_3)Cl] with [*nido*-$C_2B_9H_{12}]^-$ by ^{31}P NMR spectroscopy showed **1** to be the primary intermediate in the formation of **2**. GC–MS analysis of recovered solvent showed equimolar amounts of cyclooctene and 1,3-cyclooctadiene. A plausible mechanism for this reaction is

(15) Molecular models constructed with a locally edited version of DRILL, supplied by V. W. Day, University of Nebraska, Lincoln, NB.
(16) (a) Bondi, A. *J. Phys. Chem.* **1964**, *68*, 441. (b) Allinger, N. L.; Hirsch, J. A.; Miller, M. A.; Tyminski, I. J.; Van-Catledge, F. A. *J. Am. Chem. Soc.* **1968**, *90*, 1199.
(17) Hawthorne, M. F.; Callahan, K. P.; Wiersema, R. J. *Tetrahedron* **1974**, *30*, 1795.
(18) Albright, T. A.; Hoffman, R. *Chem. Ber.* **1978**, *111*, 1578.
(19) (a) Mingos, D. M. P. *J. Chem. Soc., Dalton Trans.* **1977**, 602. (b) Mingos, D. M. P.; Minshall, P. C.; Hursthouse, M. B.; Malik, K. M. A.; Willoughby, S. D. *J. Organomet. Chem.* **1979**, *181*, 169. (c) Mingos, D. M. P.; Forsyth, M. I.; Welch, A. J. *J. Chem. Soc., Chem. Commun.* **1977**, 605. (d) Mingos, D. M. P.; Forsyth, M. I.; Welch, A. J. *J. Chem. Soc., Dalton Trans.* **1978**, 1363.

Scheme I

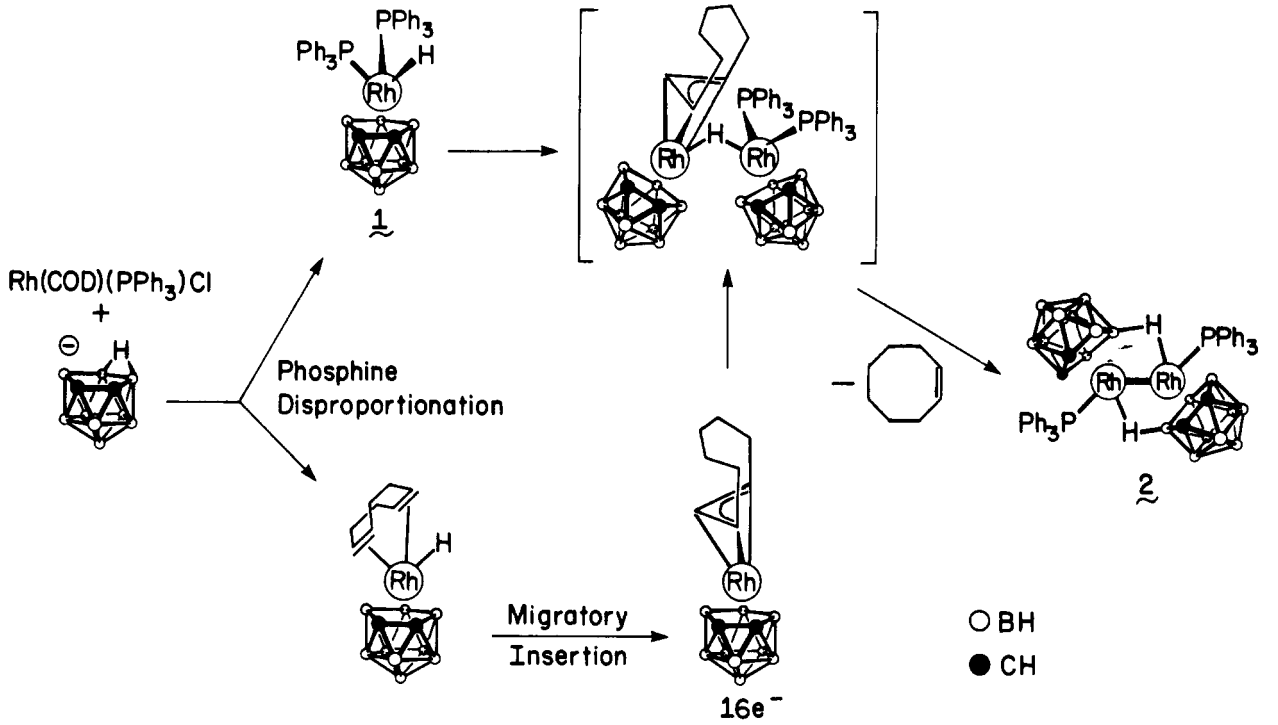

shown in Scheme I. Important aspects of this mechanism include a phosphine ligand disproportionation prior, or subsequent, to oxidative addition of the bridging B–H–B of the carborane ligand, yielding 1 equiv of **1** and a rhodacarborane formally containing a coordinated cyclooctadiene and hydride ligand derived from the bridging proton of the carborane. Migratory insertion of the hydride into the COD ligand would result in a 16-electron intermediate depicted in Scheme I. The requirement of a vacant coordination site for binuclear reductive elimination was first proposed by Norton[20] who proposed the elimination to occur via coordination of a metal hydride by an unsaturated metal alkyl (eq 5).

$$L_nM\text{-}H + ML_{n-1}\text{-}R \longrightarrow L_nM\text{---}ML_{n-1} \xrightarrow{-RH} L_nM\text{-}ML_{n-1} \quad (5)$$

In this case, coordinative unsaturation of *one* intermediate results from phosphine disproportionation yielding **1** and the 16e⁻ cyclooctenyl complex (Scheme I). Coordination of the metal hydride by this 16e⁻ intermediate, bringing both alkyl and hydride ligands into the same coordination sphere (Scheme I), precedes binuclear reductive elimination producing **2**. Primary evidence for this type of mechanism is derived from the characterization of **8** (Figure 4). The structure of **8** can be viewed as containing *both* intermediates proposed in Scheme I for the formation of **2**. Half the molecule **8** consists of a 2,1,8 analogue of **1**, resulting from phosphine ligand disproportionation from [Rh(COD)-(PEt_3)Cl] followed by polyhedral rearrangement. The other half contains a RhC_2B_9 cluster coordinated to a η^3-cyclooctenyl ligand analogous to the 16-electron intermediate proposed in Scheme I. This fragment achieves coordinative saturation via interaction with an exopolyhedral B–H on the adjacent rhodacarborane cluster.

Apparently, polyhedral rearrangement (yielding **8**) competes with binuclear elimination of cyclooctene resulting in formation of **3**. Polyhedral rearrangement precludes the possibility of interaction of the rhodium bearing the cyclooctenyl ligand with the rhodium hydride, thereby blocking reductive elimination and metal–metal bond formation. Additional precedent for this mechanism is the observation of the rearrangement of [1,2-$(CH_3)_2$-3,3-η^4-(COD)-3,1,2-$RhC_2B_9H_9$]⁻ to a stable 16-electron η^3-cyclooctenyl species upon protonation,[21] analogous to that proposed in Scheme I.

The observation of phosphine disproportionation prior to metal–metal bond formation is not limited to the reaction of [Rh(COD)(PR_3)Cl] with [*nido*-$C_2B_9H_{12}$]⁻ discussed above. We have recently discovered a quantitative preparation of **2** from the hydrogenolysis of [*closo*-3-(PPh_3)-3,3-η^2-(CH_3COO)-3,1,2-$RhC_2B_9H_{11}$] (eq 6).[22] Monitoring of this reaction (in situ) by

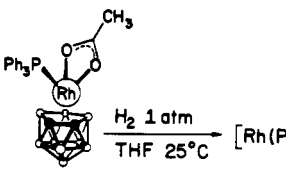

(6)

$^{31}P\{^1H\}$ NMR spectroscopy reveals **1** to be the only observed intermediate.[23] Furthermore, analogous systems which are not observed to disproportionate, notably [*closo*-2-(PPh_3)-2-(H)-2,1,7-$RhC_2B_9H_{11}$][24] and [*closo*-3-(PPh_3)-3-(H)-3,1,2-$IrC_2B_9H_{11}$],[25] fail to form products which contain metal–metal bonds. The apparent requirement of phosphine disproportionation for metal–metal bond formation in these systems may be rationalized as necessary for the creation of an open coordination site required for binuclear reductive elimination.

Experimental Section

All reactions were performed with use of Schlenk techniques under dinitrogen or argon. Solvents were purified by conventional methods and distilled from appropriate drying agents immediately before use. Rh-(COD)(RP_3)Cl,[26] [*nido*-7,8-$C_2B_9H_{12}$]⁻,[27] [Rh$(PEt_3)C_2B_9H_{10}]_2$,[6] and

(20) Norton, J. R. *Acc. Chem. Res.* **1979**, *12*, 139.

(21) Speckman, D. M.; Knobler, C. B.; Hawthorne, M. F. *Organometallics*, in press.
(22) King, R. E., III Ph.D. Dissertation, UCLA, 1982.
(23) Soto, J., UCLA, personal communication.
(24) King, R. E., III, UCLA, personal communication.
(25) Doi, J. A. Ph.D. Dissertation, UCLA, 1980.
(26) (a) Chatt, J.; Venanzi, L. M. *J. Chem. Soc.* **1957**, 4735. (b) Bennett, M. A.; Wilkinson, G. *J. Chem. Soc.* **1961**, 1418.
(27) Wiesbock, R. A.; Hawthorne, M. F. *J. Am. Chem. Soc.* **1964**, *86*, 1642.

Table VI. Details of Crystallographic Data Collection

compound	**2**	**3**	**5**	**8**
temp, K	113	298	298	298
cryst size, mm	0.11 × 0.15 × 0.40	0.20 × 0.30 × 0.30	0.29 × 0.39 × 0.10	0.40 × 0.20 × 0.15
diffractometer	Syntex $P\bar{1}$	Picker FACS-1	Syntex $P\bar{1}$	Syntex $P\bar{1}$
radiation	Mo Kα	Mo Kα	Mo Kα	Mo Kα
Space group	$P\bar{1}$	$P2_1/c$	$P2_1/c$	$P2_1/n$
a, Å	11.118 (2)	11.153 (6)	18.035 (6)	14.043 (7)
b, Å	13.456 (3)	15.228 (9)	13.156 (4)	32.638 (13)
c, Å	18.390 (3)	18.844 (10)	26.905 (8)	10.059 (4)
α, deg	93.09 (2)	90.00 (2)	90.00 (2)	90.00 (2)
β, deg	76.22 (1)	91.83 (2)	113.34 (2)	98.98 (3)
γ, deg	76.90 (2)	90.00 (2)	90.00 (2)	90.00 (2)
V, Å^3	2585.7	3198.8	5861.3	4553.9
Z	2	4	4	4
ρ(calcd), g cm^{-3}	1.36	1.46	1.40	1.32
ρ(measd), g cm^{-3}	1.32 (25 °C)	1.47	1.40	1.35
μ(calcd), cm^{-1}	7.90	11.26	7.35	8.06
scan width, deg	1.0 below Kα_1 − 1.0 above Kα_2	2.2(1 + 0.692 tan θ)	1.0 below Kα_1 − 1.0 above Kα_2	1.0 below Kα_1 − 1.0 above Kα_2
rflns measured	6388	4573	11578	7803
2θ range, deg	2–44	2–45	2–50	2–48.3
unique data	5535 > 3$\sigma(I)$	3003 > 3$\sigma(I)$	7361 > 3$\sigma(I)$	3730 > 3$\sigma(I)$
no. of parameters	307	323	359	425

[7-(7′-*nido*-7′,8′-$C_2B_9H_{11}$)-*nido*-7,8-$C_2B_9H_{11}$]$_2$[2-28] were synthesized according to literature procedures. ^{1}H and ^{31}P FTNMR measurements were made on a Bruker WP-200 spectrometer at 200.133 and 81.02 MHz, respectively, and referenced to residual isotopic resonances in the solvent (^{1}H) or external D_3PO_4 (^{31}P) according to a published procedure.[11] ^{11}B FTNMR spectra were recorded at 126.7 MHz, employing an instrument constructed by Prof. F. A. L. Anet of this department. GC–MS analyses were performed on a Perkin-Elmer Sigma 3-Kratos MS 25 instrument. Elemental analyses were performed by Schwarzkopf Laboratories, Woodside, NY. Melting points are uncorrected.

Preparation of [Rh(PPh$_3$)C$_2$B$_9$H$_{11}$]$_2$ (2). The complex [Rh(η^4-1,5-C_8H_{12})Cl]$_2$ (325 mg, 0.76 mmol) and PPh_3 (410 mg, 1.56 mmol) were dissolved in 10 mL of CH_2Cl_2 and stirred for 10 min. The solvent was removed and Tl[*nido*-7,8-$C_2B_9H_{12}$] (540 mg, 1.60 mmol) and 200 mL of THF were added to the residue. The reaction was refluxed 3 days, cooled to room temperature, and filtered through Celite. Evaporation of solvent followed by purification of the residue by column chromatography (silica gel) via elution with benzene–heptane (1:2) yielded 650 mg of **2** as dark purple crystals (86%).

Synthesis of [Rh(PPh$_3$)C$_2$B$_9$H$_{10}$C$_6$H$_5$]$_2$ (5). A 250-mL Schlenk flask was charged with [Rh(COD)Cl]$_2$ (1.00 g, 4.06 mmol), PPh_3 (1.06 g, 4.06 mmol), and CH_2Cl_2. The solution was stirred for 10 min, and solvent was removed under vacuum. $(Me_4N)^+$(*nido*-7-C_6H_5-7,8-$C_2B_9H_{11}$)$^-$ (1.26 g, 4.47 mmol) was added as a solid followed by 120 mL of MeOH, and the reaction was refluxed with stirring for 40 h, resulting in the formation of an aqua-colored precipitate. The crude product was isolated and purified by chromatography on silica gel. The band eluting with benzene was collected and concentrated by rotary evaporation, resulting in the isolation of 283 mg of **5** as black microcrystals (0.106 mmol, 12%, mp 255–260 °C): ^{31}P{^{1}H} NMR (10% C_6H_6/THF) 17.6 ppm (J_{Rh-P} = 134 Hz); ^{1}H NMR (CD_2Cl_2) 7.54–7.04 (m, 40 H, –C_6H_5), 2.71, 2.35 (br s, 2 H, carborane C–H), –8.5 ppm (very br, 2 H, Rh–H–B); ^{11}B{^{1}H} NMR ($CDCl_3$) 6.3 (2 B), –13.6 (2 B), –19.2 (3 B), –21.5 (2 B), –29.0 (4 B), –32.2 (3), –35.5 ppm (2 B).

Preparation of [Rh(PMe$_2$Ph)C$_2$B$_9$H$_{11}$]$_2$ (6). In a synthesis analogous to the preparation of **2**, [Rh(COD)Cl]$_2$ (325 mg, 0.76 mmol), PMe_2Ph (216 mg, 1.56 mmol), and Cs^+[*nido*-7,8-$C_2B_9H_{12}$]$^-$ (426 mg, 1.60 mmol) were reacted in refluxing THF (200 mL). Chromatography of the residue (silica gel) by elution with benzene–heptane (1:1) followed by concentration of the solvent resulted in the isolation of 470 mg of **6** as dark purple crystals (83%, mp 170–180 °C): ^{31}P{^{1}H} NMR 8.1 (d, J_{Rh-P} = 161 Hz), 7.1 (dd, J_{Rh-P} = 165 Hz, $^3J_{P-P}$ = 10 Hz), 1.2 pm (d, J_{Rh-P} = 130 Hz); ^{1}H NMR($CDCl_3$) 7.3 (m, 10 H, C_6H_5), 3.35, 3.37, 3.29, 2.31 (br s, 2 H, carborane C–H), 1.80–1.40 (m, 12 H, –CH_3), –8.0 ppm (br s, 2 H, Rh–H–B); ^{11}B{^{1}H} NMR($CDCl_3$) 27.2 (1 B), 22.0 (1 B), 2.3 (3 B), –1.6 (3 B), –5.3 (3 B), –9.5 (2 B), –12.5 (2 B), –18.4 (2 B), –24.9 ppm (1 B). Anal. Calcd for $C_{20}H_{44}B_9P_2Rh_2$: C, 32.16; H, 5.94; B, 26.05; P, 8.29; Rh, 27.55. Found: C, 33.94; H, 5.84; B, 26.34; P, 6.63; Rh, 27.69.

Synthesis of [Rh(PEt$_3$)C$_2$B$_9$H$_{11}$]$_2$ (7). In a preparation analogous to **2**, [Rh(COD)Cl]$_2$ (325 mg, 0.76 mmol), PEt_3 (0.23 mL, 1.56 mmol), and Cs^+[*nido*-7,8-$C_2B_9H_{12}$]$^-$ (426 mg, 1.60 mmol) were reacted in refluxing THF (200 mL). Chromatography of the residue (silica gel) by elution with benzene–heptane (1:1) followed by concentration of the eluent resulted in the isolation of **7** as dark purple crystals (410 mg, 76%, mp 230–235 °C): ^{31}P{^{1}H} NMR (10% C_6D_6/THF) 27.5 (J_{Rh-P} = 157 Hz), 25.8 (J_{Rh-P} = 160 Hz, $^3J_{P-P}$ = 8 Hz), 13.7 ppm (J_{Rh-P} = 129 Hz); ^{1}H NMR ($CDCl_3$) 3.60, 3.18, 2.80, 2.38 (br s, 2 H, carborane C–H), 1.98–1.82 (m, 12 H, –CH_2–), 1.01–0.97 (m, 18 H, –CH_3), –7.8, –9.6 ppm (br, 2 H, Rh–H–B); ^{11}B{^{1}H} NMR($CDCl_3$) 22.5, 17.5, 13.7, 6.2, 2.9, –15.6, –21.2 ppm. Anal. Calcd for $C_{16}H_{52}B_{18}P_2Rh_2$: C, 27.18; H, 7.41; B, 27.53; P, 8.76; Rh, 29.11. Found: C, 27.26; H, 7.36; B, 27.26; P, 8.76; Rh, 28.64.

Synthesis of [Rh(PEt$_3$)$_2$(H)C$_2$B$_9$H$_{10}$Rh(CODH)C$_2$B$_9$H$_{10}$] (8). A 250-mL flask was charged with 2.43 g of [Rh(COD)(PEt_3)Cl] (6.74 mmol), 1.788 g of **4** (3.37 mmol), and 100 mL of THF. The reaction was refluxed 2 days, turning dark blue-green. The solvent was removed under vacuum and the residue separated by column chromatography on silica gel. The band eluting with toluene–heptane (3:1) was collected and reduced in volume, resulting in the precipitation of 0.547 g of **3** as black microcrystals (0.78 mmol, 23%). Elution with CH_2Cl_2 resulted in the collection of a red band which yielded 0.524 g of red crystals upon concentration (0.64 mmol, 19%, mp 147–155 °C dec): ^{31}P{^{1}H} NMR (10% C_6D_6/THF) 26.9 ppm (J_{Rh-P} = 104 Hz); ^{1}H NMR (CD_2Cl_2) 5.89 (q, 2 H, J = 7 Hz), 4.47 (tr, 1 H, J = 7 Hz), 1.97–1.55 (m, 22 H, –CH_2–), 1.22–0.99 (m, 18 H, –CH_3), –10.54 ppm (d tr, 1 H, J_{Rh-P} = 18 Hz, J_{P-H} = 28 Hz); ^{11}B{^{1}H} NMR (THF) 21.0 (1 B), 2.8 (3 B), –2.6 (3 B), –5.0 (2 B), –7.2 (1 B), –12.3 (1 B), –14.1 (3 B), –16.4 (3 B), –17.9 ppm (1 B).

Photolysis of 2. A sealed 10-mm NMR tube containing 100 mg of **2** and 2.5 mL of C_6D_6 was photolyzed with use of a Hanovia 500 W medium pressure Hg lamp for 24 h. The ^{31}P NMR spectrum of the photolyzed sample revealed new resonances at 22.6 (J_{Rh-P} = 134 Hz) and 36.4 ppm (J_{Rh-P} = 168 Hz). Maintaining the tube in the dark resulted in conversion of these new species back to **2** with time for half-reaction of ca. 4 h at room temperature. The photostationary state employing the conditions given above represents 9% conversion of **2**.

General Methods of Crystallographic Analysis. The solution and refinement of the structure of **2** was accomplished with calculations performed on an IBM 360-91 computer with locally edited versions of HKLEDIT, JBPATT, JBFBIG, PEAKLIST, ORFLS, DATRED, RBANG, and ORFFE. All other calculations were performed on the UCLA Chemistry Department DEC VAX 11/780 with the UCLA crystallographic package (locally edited versions of CARESS, PROFILE, ORFLS, ORFFE, and ORTEP). Observed intensities were reduced to the relative square amplitudes, $[F_o]^2$, by means of Lorentz and polarization corrections. Details of individual data collections are summarized in Table VI. Scattering factors for H were obtained from Stewart et al.[29] and for other atoms were taken from the "International Tables for X-ray Crystallography", Volume IV.[30] Anomalous dispersion terms[31] were applied to scattering of Rh, Cl, and P.

(28) Hawthorne, M. F.; Owen, D. A.; Wiggins, J. W. *Inorg. Chem.* **1971**, *10*, 1304.

(29) Stewart, R. F.; Davidson, E. R.; Simpson, W. T. *J. Chem. Phys.* **1965**, *42*, 3175.

(30) "International Tables for X-ray Crystallography"; Kynoch Press: Birmingham, England, 1974; Vol. IV.

(31) Cromer, D. T. *Acta. Crystallogr.* **1965**, *18*, 17.

X-ray Crystallographic Analysis of 2. A crystal of **2** suitable for X-ray analysis was grown from CH_2Cl_2/heptane, mounted on a glass fiber, and covered with a thin layer of epoxy glue to prevent loss of solvate. Preliminary photographs indicated the crystal to be triclinic, space group $P\bar{1}$. Data were collected on a Syntex $P\bar{1}$ autodiffractometer at 113 °K; details of the collection are given in Table VI.

The positions of the rhodium and phosphorus atoms were obtained from the Patterson synthesis. All remaining atoms, including hydrogen atoms, were located in subsequent difference Fourier maps. The C_6H_5 rings of the triphenylphosphine ligands were constrained as rigid groups with C–C = 1.39 Å and C–H = 1.0 Å. All remaining hydrogen atoms were refined isotropically with arbitrary temperature factors (B) of 2.0. The rhodium, phosphorus, and chlorine atoms (CH_2Cl_2 solvate) were refined anisotropically along with the occupancy of the two CH_2Cl_2 solvate molecules which converged at 0.674 (8) and 0.495 (11). The refinement converged at $R = 0.047$ and $R_w = 0.072$.[32] Final positional parameters and isotropic and anisotropic temperature factors are listed in Tables S.1 and S.2 as supplementary material.

X-ray Crystallographic Analysis of 3. Crystals suitable for an X-ray crystallographic study were grown by layering a toluene solution of **3** with heptane. Weissenberg photographs revealed the crystal to belong to the monoclinic system, space group $P2_1/c$. Details of the data collection are presented in Table VI. The position of the rhodium and phosphorus atoms were deduced from a Patterson synthesis. All remaining atoms, including hydrogen atoms, were located in subsequent difference Fourier maps. The rhodium, phosphorus, and terminal carbons on the PEt_3 ligands were refined anisotropically, and the remaining non-hydrogen atoms were refined isotropically. The positions of the hydrogen atoms were refined and assigned an arbitrary temperature factor (B) of 5.00.

Least-squares refinement converged to $R = 0.032$ and $R_v = 0.038$.[32] Final positional and thermal parameters are listed in Tables S.3 and S.4 as supplementary material.

X-ray Crystallographic Analysis of 5. Crystals of *5* suitable for crystallographic analysis were grown from CH_2Cl_2 by layering the solution with heptane. Preliminary Weissenberg photographs showed the crystal to be monoclinic, space group $P2_1/c$. Data were collected at 298 K on a Syntex $P\bar{1}$ autodiffractometer. Details of the data collection are summarized in Table VI.

The positions of the rhodium and phosphorus atoms were deduced from a Patterson synthesis. Subsequent difference Fourier maps were employed in the location of all non-hydrogen atoms, including the disordered CH_2Cl_2 solvate. The hydrogen atoms of the carborane cage and phenyl rings were included in calculated positions, assuming idealized geometries and bond distances (C–H = 0.90 Å, B–H = 1.10 Å). Final least-squares refinement cycles employed anisotropic temperature factor refinement of the rhodium, phosphorus, and chlorine atoms. The positions of the hydrogen atoms were not refined and were assigned arbitrary isotropic temperature factors (B) of 3.50.

Refinement of the structure resulted in convergence at $R = 0.051$ and $R_w = 0.062$.[32] Final positional and temperature factor data are listed in Tables S.5 and S.6 as supplementary material.

X-ray Crystallographic Analysis of 8. Single crystals of **8** were obtained from a layered toluene/ethanol solution. At 20 °C, crystals of **8**·$CH_3C_6H_5$ are monoclinic, space group $P2_1/n$ (an alternate setting of $P2_1/c$). Data were collected with a Syntex $P\bar{1}$ autodiffractometer at 298 K. Details of the data collection are given in Table VI.

The heavy-atom technique, difference Fourier syntheses, and full-matrix least-squares refinement were employed to solve and refine the structure, resulting in the locations of all non-hydrogen atoms. The positional coordinates for the carborane hydrogen atoms and cyclooctenyl ligand hydrogen atoms wre generated by using idealized geometry and 0.95 Å C–H and 1.15 Å B–H bond distances. All hydrogen atoms were held fixed in subsequent refinement cycles and assigned arbitrary isotropic temperature factors (B) of 7.0. The toluene solvate was located in difference maps and was refined as a rigid group employing a C–C distance of 1.395 Å, a C–CH_3 distance of 1.470 Å, and a C–H distance of 0.95 Å. A single isotropic temperature factor was used for the group which converged at $B = 11.7$.

Final cycles of least-squares refinement utilized anisotropic temperature factors for the rhodium, phosphorus, boron, and carbon atoms (excluding solvate), resulting in a convergence at $R = 0.068$ and $R_w = 0.079$.[32] Final positional and temperature factor data are listed in Tables S.7 and S.8 as supplementary material.

Acknowledgment. We thank Susan Heytens for the illustrations and Warren Powell of the Chemical Abstracts Service for naming the complexes. We gratefully acknowledge the Basic Science Division of the Department of Energy for support under Grant DE-ATO3-80 ER10673 and the National Science Foundation Grant CHE 77-22910 for the purchase of the Digital VAX-11/780 computer and CHE 77-05926 for the purchase of the Bruker WP-200 FTNMR spectrometer.

Registry No. 2, 68914-09-0; **3**, 87088-22-0; **4**, 79830-46-9; **5**, 94294-04-9; **6**, 94294-05-0; **7**, 94323-90-7; **8**, 94323-91-8; Tl[*nido*-7,8-$C_2B_9H_{12}$], 94234-91-0; $(Me_4N)^+$[*nido*-7-C_6H_5-7,8-$C_2B_9H_{11}$]$^-$, 39336-45-3; Cs^+-[*nido*-7,8-$C_2B_9H_{12}$]$^-$, 63748-65-2; [Rh(η^4-1,5-C_8H_{12})Cl]$_2$, 12092-47-6; [Rh(COD)(PEt_3)Cl], 31943-93-8; PPh_3, 603-35-0; PMe_2Ph, 672-66-2; PEt_3, 554-70-1; Rh, 7440-16-6.

Supplementary Material Available: Tables of observed and calculated structure factors and tables (S.1–S.8) of final positional and thermal parameters for **2**, **3**, **5**, and **8** (98 pages). Ordering information is given on any current masthead page.

(32) $R = \sum||F_o| - |F_c||/\sum|F_o|$, $R_w = \sum w(|F_o| - |F_c|)^2/\sum wF_o^2$, $w = 1/\sigma^2(F_o)$.